Biased Star Tracker Measurements of Forty-Nine Stars from Flight Data

Noah H. Smith,* Sungkoo Bae,† and Bob E. Schutz‡
University of Texas at Austin, Austin, Texas 78712

Approximately 1% of the 10,000 stars observed by the ice, cloud, and land elevation satellite star trackers are believed to have position measurement biases caused by near-neighbor stars. The biases are in the tracker measurements, not the star catalogs. Empirical biases were derived for 49 stars. A survey was performed to detect and characterize biased stars by treating each observed star as a target, predicting the tracker measurements of the target, and then comparing the observations and predictions. The distribution of prediction accuracies for unbiased stars had a mean of 1.46 arcseconds and a standard deviation of 0.61 arcseconds. Ninety percent of the sky was covered and five million passes of 10,472 stars were processed. Stars were classified using a Mahalanobis distance parameter, which scaled position residuals by prediction uncertainties. Stars with large Mahalanobis distances were then studied individually.

Nomenclature

d	=	unitless scalar Mahalanobis distance of position residual
f	=	tracker focal length, mm
$\mathbf{H}$	=	2×3 sensitivity matrix, arcsec^2/rad^2
h, v	=	horizontal and vertical coordinates of a star on the tracker focal plane, arcsec
k	=	scaling factor, arcsec/rad
$\mathbf{P}$	=	3×3 attitude estimate covariance, rad^2
$\mathbf{p}$	=	2×1 target star observed position in the tracker frame, arcsec
$\mathbf{p}_{\text{predict}}$	=	2×1 target star predicted position in the tracker frame, arcsec
$\mathbf{R}$	=	2×2 target star noise covariance matrix, arcsec^2
$\mathbf{r}$	=	2×1 position residual in the tracker frame, arcsec
$\mathbf{S}$	=	2×2 position covariance matrix, arcsec^2
$\mathbf{u}$	=	3×1 unit vector of a star position in the tracker frame
x, y	=	coordinates of a star on the tracker focal plane, mm
$\delta\boldsymbol{\theta}$	=	2×1 perturbation of tracker frame, rad
$\delta\mathbf{r}$	=	2×1 perturbation of position residual, arcsec
$\delta\mathbf{u}$	=	3×1 perturbation of unit vector of a star direction
$\delta h, \delta v$	=	perturbation of horizontal and vertical coordinates, arcsec
$\Theta_{h,v}$	=	angular coordinates of a star in the tracker frame, rad

I. Introduction

THE ice, cloud, and land elevation satellite (ICESat) star trackers are commercial off-the-shelf (COTS) models, an HD-1003 and two CT-602s. For some stars, tracker position measurements are biased by unresolved near-neighbor stars that blend with the target star image [1,2]. The biases are in the tracker measurements, not the star catalog positions. Biased position measurements are a problem for both star identification and attitude estimation because both methodologies compare measured and catalog positions. There are

descriptions in the literature of analyzing star catalogs for near-neighbor stars that could cause star tracker measurement errors [1,3]. This paper focuses on using flight data to estimate empirical corrections.

Mission catalogs typically remove stars that are too faint or bright to be tracked and attempt to remove or correct stars with potential biases. The SKY2000 Master Catalog is a common starting point for creating mission catalogs. Astronomical missions using faint guide stars work directly with large astronomical catalogs [4]. Some European missions work with the catalogs produced by the Hipparcos astrometry mission [5]. SKY2000 does not contain all of the stars typical trackers can acquire, or all of the near-neighbors that can effect target stars. The term "blended position" has been used for catalog records which represent the apparent centroid of a group of stars [2,6]. The SKY2000 catalog includes analytically derived blended positions for some near-neighbor cases. Records with blended positions are indicated by a binary flag [7]. In typical COTS trackers, each image pixel covers about an arcminute of the sky and the star images are defocused to cover multiple pixels for centroiding with an accuracy of a few arcseconds. If a neighboring star is within a few arcminutes of a target star their light peaks overlap on the image pixels. The near-neighbor can alter the apparent centroid of the target and bias its measured position. Other types of bias besides static blended positions are possible. If the group members are intermittently resolved or include variable stars the blended position can vary with time, such cases have been called *ping-pong stars* [2,5]. Analytic prediction of blended position centroids is difficult because of uncertainties in the instrument magnitudes of group members. The 2004 Aura mission catalog is of interest because of the work done on predicting near-neighbor effects (the results were later incorporated in the SKY2000 catalog). For the 3542 stars in the Aura onboard catalog, near-neighbors within three arcminutes were analytically combined into blended positions based on the defocusing of CT-602 type trackers [1]. Of the 49 biased stars described in this paper, four appear in the Aura onboard catalog. These four stars were processed identically to the other 45 stars and their descriptions are based on the same standard SKY2000 catalog. They are listed separately for possible comparison with Aura onboard catalog results.

ICESat was launched on 13 January 2003 into a near-circular, frozen orbit with an altitude of approximately 600 km and an inclination of 94°. The science instrument is the Geoscience Laser Altimeter System (GLAS). ICESat carries four star trackers. The Instrument Star Tracker (IST) is an HD-1003. It has an $8° \times 8°$ field of view, instrument magnitude 6.2 sensitivity, a 512×512 pixel CCD, and tracks up to 6 stars with 10 Hz sampling. The IST tracks any available stars in the field of view. The Laser Reference Sensor (LRS) is a second, modified 10 Hz HD-1003 with third-party optics and baffle reducing the field of view to $0.5° \times 0.5°$ and increasing the

*Doctoral Candidate, Center for Space Research. Member AIAA.
†Research Scientist/Engineer, Center for Space Research. Member AIAA.
‡Professor and Associate Director, Center for Space Research. Associate Fellow AIAA.

sensitivity to instrument magnitude 7.5. LRS data is not discussed in this paper due to its small field of view. GLAS also includes hemispherical resonating gyros sampled at 10 Hz. The two CT-602 bus star trackers (BST1 and BST2) point 30° to either side of the IST. They both have an $8° \times 8°$ field of view, 10 Hz sampling rate, instrument magnitude 7.1 sensitivity, 512×512 pixel CCD, and track five stars simultaneously. The BSTs use star position predictions from the flight computer to acquire stars specified in an onboard mission catalog [2,8].

II. Star Tracker Position Measurements and Errors

Horizontal and vertical coordinates on the focal plane (or sometimes defined on the field of view) were used to represent a star position. They can be expressed using f, x, and y:

$$h = k(x/f) \tag{1}$$

$$v = k(y/f) \tag{2}$$

An equivalent expression uses similar triangles and $\mathbf{u}$ components:

$$h = k(u_1/u_3) \tag{3}$$

$$v = k(u_2/u_3) \tag{4}$$

The HD-1003 outputs horizontal and vertical coordinates. The CT-602s output angular coordinates:

$$\Theta_h = \tan^{-1}(u_1/u_3) = \tan^{-1}(h/k) \tag{5}$$

$$\Theta_v = \tan^{-1}(u_2/u_3) = \tan^{-1}(v/k) \tag{6}$$

A star position $\mathbf{u}$ has a simple expression in terms of horizontal and vertical coordinates or angular coordinates. For horizontal and vertical coordinates, trigonometric functions are not involved:

$$u'_1/1 = \tan \Theta_h = h/k \tag{7}$$

$$u'_2/1 = \tan \Theta_v = v/k \tag{8}$$

$$\mathbf{u}' = [u'_1 \quad u'_2 \quad 1]^T \tag{9}$$

$$\mathbf{u} = \mathbf{u}'/\|\mathbf{u}'\| \tag{10}$$

Tracker errors can be classified as low spatial frequency error, high spatial frequency error, and noise [9]. High spatial frequency error covers variations on the scale of the image pixels. For the ICESat trackers this is a 3–4 Hz zero-mean variation with amplitude of about an arcsecond and is not explicitly corrected. It may be useful to include a fourth class of tracker error for identification of stars. Star identification is generally based on a search for a catalog star near a measured star [10]. For a measured star with near-neighbors, it may be better to identify multiple catalog stars and determine if they caused measurement errors. Another class of errors may be needed for timing, timestamp, and data gap issues [11].

Figure 1 shows the low spatial frequency error corrections for the IST. The corrections for BST1 and BST2 are similar. Low spatial frequency error includes position variations that occur on scales larger than the pixel size. Corrections for low spatial frequency errors were applied to all tracker measurements. These corrections were at most a few arcseconds. The corrections were estimated by fitting polynomials of h and v to the position errors [12].
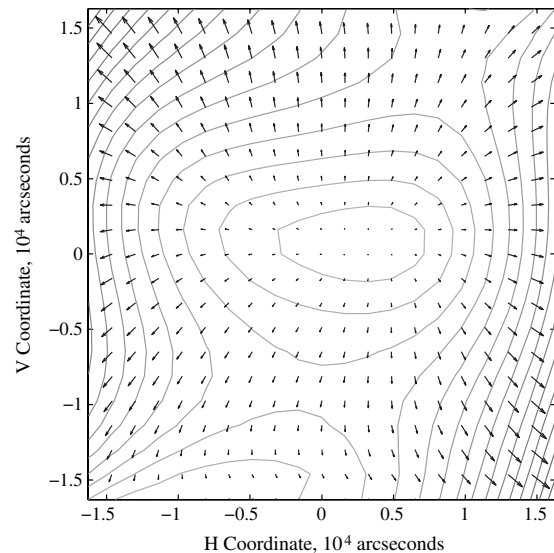

Fig. 1 Low spatial frequency error corrections of up to 2.5 arcseconds for the IST field of view.
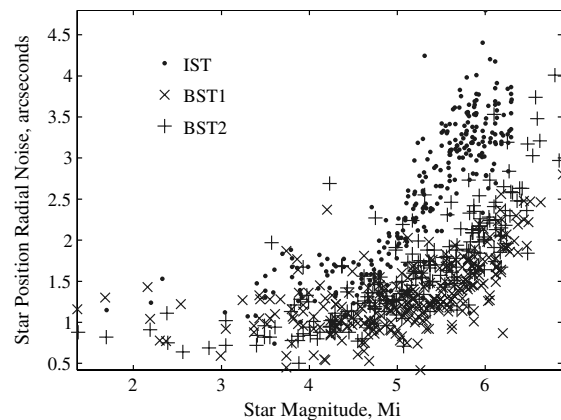

Fig. 2 Radial position noise estimates versus star brightness.

Figure 2 shows the estimated noise versus magnitude for the three trackers. The estimates are larger for the IST than for the other two trackers. Noise estimation was based on the observed variations of the angular separations between pairs of stars [5]. The variance of the angular separation between two stars is equal to the sum of their individual angular variances. Given measurements of two stars, the variance of their angular separation can be calculated directly. For measurements of three stars, variances can be calculated for the angular separations of the three possible pairings of stars. Three equations can be formed and solved for the three unknown individual variances. When there are more than three stars, there can be a variable number of simultaneously measured pairs of stars and angular separations. If there are more simultaneously measured pairs than there are stars, the resulting system of equations is over-determined and can be solved using least squares.

III. Biased Star Detection

Each star measured by the trackers was processed separately. When a star was being processed it was designated the target star. The set of measurements of the target star as it moved across the tracker field of view was designated the target star pass. Attitude estimation was performed using other stars in the field of view so that if the target star measurements were biased they would not bias the attitude estimate.

A. Position Residual r

All position vectors and covariance matrices from all measurement times in the target star pass were expressed in the midpass tracker frame using rotational transformations. The midpass tracker coordinate frame was defined by the tracker attitude estimate at the midpoint in time of the target star pass. Because the midpass tracker frame was constant in inertial space, the predicted position of the target star expressed in the midpass tracker frame was constant. Errors in the measurements and attitude estimates produced variations in the target star measured positions when expressed in the midpass tracker frame. The position residuals were the difference of the measured and predicted positions expressed in the midpass tracker frame using horizontal and vertical coordinates:

$$\mathbf{r} = \mathbf{p} - \mathbf{p}_{\text{predict}} \qquad (11)$$

B. Position Covariance S

Covariances for all measurement times in the target star pass were expressed in the midpass tracker frame using horizontal and vertical coordinates. The covariances described the variation of two state variables: the horizontal and vertical coordinate position of the target star expressed in the midpass tracker frame. There are two types of covariances to consider, $\mathbf{P}$ and $\mathbf{R}$. $\mathbf{P}$ is discussed first, the transformation of 3×3 $\mathbf{P}$ covariances to 2×2 covariances is described below. Finally, $\mathbf{P}$ and $\mathbf{R}$ are added to form the overall position covariance $\mathbf{S}$.

The 3×3 $\mathbf{P}$ covariances were calculated using single-frame vector observation attitude estimation methods [13]. A sensitivity matrix $\mathbf{H}$ was derived such that $\mathbf{H}\mathbf{P}\mathbf{H}^{\mathbf{T}}$ was a 2×2 covariance expressed in the midpass tracker frame using horizontal and vertical coordinates. $\mathbf{H}$ gave the change $\delta\mathbf{r}$ resulting from a perturbation $\delta\boldsymbol{\theta}$ of an attitude estimate:

$$\delta\mathbf{r} = \mathbf{H}\delta\boldsymbol{\theta} \qquad (12)$$

To form $\mathbf{H}$, a matrix giving the change $\delta\mathbf{u}$ of the first two $\mathbf{u}$ components was derived (the third component was not needed). The unit vector components before the perturbation were $\mathbf{u_0}$:

$$\delta\mathbf{u} = \mathbf{u} - \mathbf{u_0} = [\, u_1 - u_{10} \quad u_2 - u_{20} \,]^T \qquad (13)$$

A rotation matrix for a 1-2-3 rotation sequence was used to derive expressions for $\delta\mathbf{u}$:

$$\begin{bmatrix} u_1 \\ u_2 \\ u_3 \end{bmatrix} = \begin{bmatrix} c\theta_2 c\theta_3 & c\theta_1 s\theta_3 + s\theta_1 s\theta_2 c\theta_3 & s\theta_1 s\theta_3 - c\theta_1 s\theta_2 c\theta_3 \\ -c\theta_2 s\theta_3 & c\theta_1 c\theta_3 - s\theta_1 s\theta_2 s\theta_3 & s\theta_1 c\theta_2 + c\theta_1 s\theta_2 s\theta_3 \\ s\theta_2 & -s\theta_1 c\theta_2 & c\theta_1 c\theta_2 \end{bmatrix} \begin{bmatrix} u_{10} \\ u_{20} \\ u_{30} \end{bmatrix} \qquad (14)$$

The change of the first unit vector component was derived by substituting in the small perturbation $\delta\boldsymbol{\theta}$ and neglecting higher-order terms:

$$u_1 = (c\delta\theta_2 c\delta\theta_3)u_{10} + (c\delta\theta_1 s\delta\theta_3 + s\delta\theta_1 s\delta\theta_2 c\delta\theta_3)u_{20} + (s\delta\theta_1 s\delta\theta_3 - c\delta\theta_1 s\delta\theta_2 c\delta\theta_3)u_{30} \qquad (15)$$

$$u_1 = u_{10} + (\delta\theta_3 + \delta\theta_1 \delta\theta_2)u_{20} + (\delta\theta_1 \delta\theta_3 - \delta\theta_2)u_{30} \qquad (16)$$

$$\delta u_1 = [\, 0 \quad -u_{30} \quad u_{20} \,]\delta\boldsymbol{\theta} \qquad (17)$$

The change of the second unit vector component was derived in the same way:

$$u_2 = (-c\delta\theta_2 s\delta\theta_3)u_{10} + (c\delta\theta_1 c\delta\theta_3 - s\delta\theta_1 s\delta\theta_2 s\delta\theta_3)u_{20} + (s\delta\theta_1 c\delta\theta_2 + c\delta\theta_1 s\delta\theta_2 s\delta\theta_3)u_{30} \qquad (18)$$

$$u_2 = (-\delta\theta_3)u_{10} + (1 - \delta\theta_1 \delta\theta_2 \delta\theta_3)u_{20} + (\delta\theta_1 + \delta\theta_2 \delta\theta_3)u_{30} \qquad (19)$$

$$\delta u_2 = [\, u_{30} \quad 0 \quad -u_{10} \,]\delta\boldsymbol{\theta} \qquad (20)$$

The two components were then combined:

$$\delta\mathbf{u} = \begin{bmatrix} 0 & -u_{30} & u_{20} \\ u_{30} & 0 & -u_{10} \end{bmatrix}\bigg|_{\mathbf{u_0}} \delta\boldsymbol{\theta} \qquad (21)$$

The functions expressing h and v coordinates were then used:

$$h = f_h(\mathbf{u}) = k(u_1/u_3) \qquad (22)$$

$$v = f_v(\mathbf{u}) = k(u_2/u_3) \qquad (23)$$

The change of the h component was derived from the Taylor series expression:

$$h(\mathbf{u}) = h(\mathbf{u_0}) + \frac{\partial f_h}{\partial \mathbf{u}}\bigg|_{\mathbf{u_0}} (\mathbf{u} - \mathbf{u_0}) + \ldots \qquad (24)$$

$$\delta h = [\, k/u_3 + ku_1^2/u_3^3 \quad ku_1 u_2/u_3^3 \,]|_{\mathbf{u_0}}\delta\mathbf{u} \qquad (25)$$

The change of the v component was derived in the same way:

$$v(\mathbf{u}) = v(\mathbf{u_0}) + \frac{\partial f_v}{\partial \mathbf{u}}\bigg|_{\mathbf{u_0}} (\mathbf{u} - \mathbf{u_0}) + \ldots \qquad (26)$$

$$\delta v = [\, ku_1 u_2/u_3^3 \quad k/u_3 + ku_2^2/u_3^3 \,]|_{\mathbf{u_0}}\delta\mathbf{u} \qquad (27)$$

The product of the coordinate changes and $\delta\mathbf{u}$ gave the sensitivity matrix:

$$\mathbf{H} = \begin{bmatrix} k/u_3 + ku_1^2/u_3^3 & ku_1 u_2/u_3^3 \\ ku_1 u_2/u_3^3 & k/u_3 + ku_2^2/u_3^3 \end{bmatrix}\begin{bmatrix} 0 & -u_3 & u_2 \\ u_3 & 0 & -u_1 \end{bmatrix}\bigg|_{\mathbf{u_0}} \qquad (28)$$

This expression for the sensitivity matrix was evaluated using the measured $\mathbf{u}$ expressed in the midpass tracker frame using horizontal and vertical coordinates.

The covariance $\mathbf{R}$ represented the tracker measurement noise for the target star expressed in the midpass tracker frame using
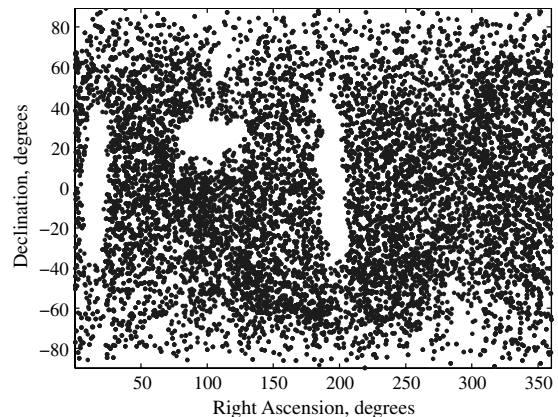

Fig. 3   Stars found in the survey [2].

Table 1   Numbers of unique stars found in the survey grouped by tracker

Tracker	Number of stars	Exclusive	IST	BST1	BST2	All
IST	9410	4903	——	244	391	3872
BST1	4755	267	244	——	292	3872
BST2	4978	305	391	292	——	3872

horizontal and vertical coordinates. The measurement noise estimates described above were used. The noise was assumed to be the same in both the horizontal and vertical directions. The noise value for a target star was converted to arcseconds and placed on the diagonal of **R**.

The overall position covariance **S** expressed in the midpass tracker frame using horizontal and vertical components was the sum of the attitude estimate and measurement noise covariances:

$$\mathbf{S} = \mathbf{HPH^T} + \mathbf{R} \qquad (29)$$

C.   Mahalanobis Distance d

Variations of the target star position residuals were described empirically by their distributions in the midpass tracker frame and analytically by their **S** covariances. The central limit theorem from probability theory states that the mean of a sufficiently large sample of independent random variables is approximately normally distributed. A large number of independent random noise errors contributed to the variations of the target star position residuals. Sample means for position residuals were assumed to be approximately normally distributed by the central limit theorem, with sample covariances related to sample sizes and **S** covariances. Sample covariances were assumed to decrease with the sample size:

$$\text{sample covariance} = \mathbf{S}/\sqrt{\text{sample size}} \qquad (30)$$

This was demonstrated by plots of position residuals. As sample sizes increased, distributions of position residuals formed sharper peaks. This principle of reducing position uncertainty by increasing the sample size is important in astrometry [14].

For an initial classification of whether a star was biased or not, its position residuals and covariances were considered together. A useful scalar parameter that combined **r** and **S** was d, the Mahalanobis distance of the residuals. The Mahalanobis distance was introduced by the statistician P. C. Mahalanobis in 1936. One of its uses is detecting multivariate outliers. Detecting outliers was the objective here, and d was used as a multivariate generalization of the ratio of a mean and a standard deviation:

Table 2   Biased stars found in the survey

SKYMAP	Hipparcos Star Catalog	Passes	BST passes	d	Residual, arcseconds	Dec. residual (arcseconds)
8190190	40817	598	——	11.50 ± 0.64	26.43 ± 1.39	18.05 ± 2.19
21570079	108378	224	2	9.41 ± 1.79	-20.99 ± 1.60	16.63 ± 5.10
21430083	107253	36	15	9.29 ± 2.45	23.82 ± 6.41	14.35 ± 2.46
21440193	107382	108	——	9.26 ± 0.74	-10.42 ± 0.90	24.96 ± 1.44
21020031	103814	415	——	9.18 ± 0.30	24.68 ± 1.51	7.36 ± 0.47
110134	967	145	14	8.74 ± 0.88	16.88 ± 1.53	19.39 ± 0.94
14240025	70400	280	21	8.39 ± 0.59	-23.90 ± 1.15	1.69 ± 0.65
16200091	80047	1925	7	7.06 ± 0.54	3.95 ± 1.80	19.85 ± 1.10
22220131	110478	513	169	6.88 ± 2.36	20.52 ± 6.61	7.50 ± 2.79
20180172	100122	57	9	6.19 ± 1.20	-7.19 ± 2.23	22.79 ± 3.57
9570131	48839	493	296	5.02 ± 0.84	14.79 ± 1.52	-4.06 ± 1.20
21440030	107310	269	14	4.52 ± 0.51	8.88 ± 1.25	10.62 ± 1.23
15240088	75411	215	——	4.43 ± 0.42	1.22 ± 0.79	-12.69 ± 0.45
310089	2484	880	880	4.30 ± 0.62	-3.14 ± 0.54	12.91 ± 1.00
14130055	69481	1331	931	3.77 ± 0.54	9.27 ± 0.98	6.15 ± 0.98
2540010	13518	1076	756	3.69 ± 0.77	3.07 ± 1.69	10.79 ± 3.10
16400088	81632	280	36	3.66 ± 0.69	-9.06 ± 2.22	5.27 ± 1.57
21420079	107162	10	——	3.64 ± 0.38	8.78 ± 1.25	-4.63 ± 1.06
3230087	15795	50	36	3.36 ± 0.47	-9.16 ± 1.25	2.79 ± 1.53
16160102	79757	348	274	3.32 ± 0.82	6.54 ± 2.49	6.33 ± 1.15
20220229	100515	43	1	3.23 ± 0.37	8.75 ± 1.24	3.47 ± 0.37
18560046	92946	26	——	3.17 ± 0.20	8.68 ± 0.65	-2.59 ± 0.37
18490160	92391	118	29	3.07 ± 0.49	2.73 ± 1.14	-8.56 ± 1.09
21010039	103734	1044	645	2.71 ± 0.68	5.51 ± 1.80	5.93 ± 2.23
4110075	19571	377	273	2.66 ± 0.46	-3.02 ± 1.58	7.21 ± 1.29
21440054	107323	1786	1317	2.53 ± 0.44	7.42 ± 1.21	0.49 ± 1.34
14260028	70574	144	84	2.52 ± 0.60	-3.09 ± 1.27	-6.89 ± 1.85
4500154	22534	117	2	2.49 ± 0.62	-5.05 ± 1.88	-4.10 ± 2.20
22550117	113222	277	180	2.43 ± 0.51	-6.72 ± 1.22	-3.62 ± 1.89
9510120	48374	1468	1223	2.28 ± 0.27	-0.80 ± 0.85	6.78 ± 0.58
19240223	95447	249	249	2.28 ± 0.37	-6.38 ± 0.95	1.70 ± 0.97
9290031	46509	319	218	2.23 ± 0.21	1.10 ± 0.98	6.30 ± 0.55
22080173	109332	478	471	2.11 ± 0.56	3.57 ± 1.29	5.00 ± 1.41
16080010	79043	261	26	2.09 ± 0.28	1.61 ± 0.72	6.07 ± 0.64
13510003	67589	1287	881	2.03 ± 0.51	5.73 ± 1.09	2.59 ± 0.92
17340102	85998	289	1	2.03 ± 0.38	-0.45 ± 1.60	-5.86 ± 1.06
20000063	98461	186	186	1.97 ± 0.37	4.53 ± 0.97	-4.48 ± 0.74
20370024	101716	201	163	1.90 ± 0.54	5.20 ± 1.67	1.69 ± 0.68
10550078	——	794	533	1.87 ± 0.24	-4.70 ± 0.81	2.40 ± 0.60
14190049	69996	1232	1104	1.85 ± 0.45	2.08 ± 0.78	-4.93 ± 1.23
21190179	——	2158	1705	1.82 ± 0.34	5.16 ± 1.02	-0.20 ± 0.85
19290088	95823	67	67	1.81 ± 0.15	4.12 ± 0.40	2.89 ± 0.24
9010159	44342	213	213	1.80 ± 0.28	-6.71 ± 2.03	1.50 ± 0.96
11270140	55945	598	411	1.79 ± 0.29	-0.08 ± 0.95	-5.34 ± 0.71
19150063	94624	262	262	1.79 ± 0.25	-5.07 ± 0.78	-0.41 ± 0.66

Table 3 Biased stars found in the survey that are also in the Aura onboard catalog

SKYMAP	HIP	Aura	Passes	BST passes	d	Residual, arcseconds	Dec. residual, arcseconds
23190077	115152	3025	238	——	15.51 ± 1.46	29.65 ± 1.92	34.99 ± 1.31
17310145	85786	759	77	——	8.28 ± 1.75	17.76 ± 4.33	-17.05 ± 4.09
14290104	70874	20	959	565	3.33 ± 0.91	-8.99 ± 1.81	2.88 ± 2.67
19370139	96536	1204	144	144	2.74 ± 0.38	3.07 ± 0.74	-7.70 ± 1.25

$$d^2 = \mathbf{r^T S^{-1} r} \qquad (31)$$

Like the ratio of a mean and a standard deviation, d is a unitless parameter indicating the statistical significance of the residuals. Stars with low uncertainties $\mathbf{S}$ and large residuals $\mathbf{r}$ were flagged for further investigation by their high d values. Target stars with large uncerxtainties $\mathbf{S}$ had smaller d values and were not initially flagged for further investigation.

IV. Survey Characteristics

Publicly available ICESat data were used for the survey. This limited sky coverage to ICESat science campaigns. The science campaigns were periods in which a GLAS laser was operating. These periods were approximately 33 days long. They were identified by a unique integer and letter combination designating the laser sources and their sequences of operation. The science campaigns used were 2a, 2c, 3b, 3f, 3g, and 3h (2a was about 45 days long). In total they covered 228 days from 2003 to 2007.

Figure 3 shows the survey sky coverage. Approximately 90% of the sky was covered and five million target star passes were individually processed. The mean target star pass time span was 78.3 ± 27.7s and included hundreds of 10 Hz measurements. The large standard deviation shows that there was a wide distribution of time spans. If a new star was acquired as it entered the field of view then its time span was longer. If a new star was acquired in the center of the field of view then its time span was shorter. The nodes of the ICESat orbit plane moved about $0.5°$ per day or $180°$ per year. The sun was near the orbit plane during campaigns 2c and 3f, creating the gap in survey coverage at $100°$ right ascension and $20°$ declination in Fig. 3. The two vertical gaps at 20 and $200°$ right ascension were areas that were not covered by the survey data.

Passes less than 10 s long were edited out because of small sample sizes. This also rejected some unusual cases such as transients (satellites, dust particles) mistaken for stars or biased stars that were only marginally being identified. After editing, the survey data included 3.4 million passes of 10,472 unique stars.

Table 1 shows the numbers of unique stars found in the survey, grouped by tracker. The trackers had two primary modes of operation: directed mode and undirected mode. In directed mode the spacecraft flight computer used an onboard attitude estimate and onboard star catalog to direct a tracker where in its field of view to acquire new stars. A result of directed mode is that only stars in the onboard star catalog are acquired and tracked. In undirected mode a tracker can acquire and track any star in its field of view. The IST operated in undirected mode and the BSTs operated in directed mode, resulting in a larger number of unique IST stars than unique BST stars.

Two hierarchical levels of statistics were computed. The lower level described individual target star passes. The higher level described an individual star by combining its lower level statistics. One version of higher level star statistics was computed using all three trackers. Additional versions were computed for each tracker alone. For all three trackers, the values of estimated position biases were very close together. The most significant differences between the trackers were sensitivity and noise. Their overall effects on position biases were small. The statistics and plots in the results section are for all three trackers unless noted. Higher level star statistics were calculated as the median values of lower level pass statistics to reduce the effects of outliers. If a star's higher level statistics for r and d were less than five arcseconds and one then the star was classified as unbiased (the Mahalanobis distance d is a unitless ratio indicating statistical significance). If a star did not meet these criteria it was flagged for additional investigation.

V. Results

The survey results are descriptions of 49 stars that have biased tracker measurements and statistics for thousands of unbiased stars. The biases are in the tracker measurements, not the star catalogs. These stars have a range of bias magnitudes and all have been visually examined to confirm the presence of a bright near-neighbor. They are described in two tables. The first table lists 45 stars. The second table lists four stars in the Aura mission onboard catalog.
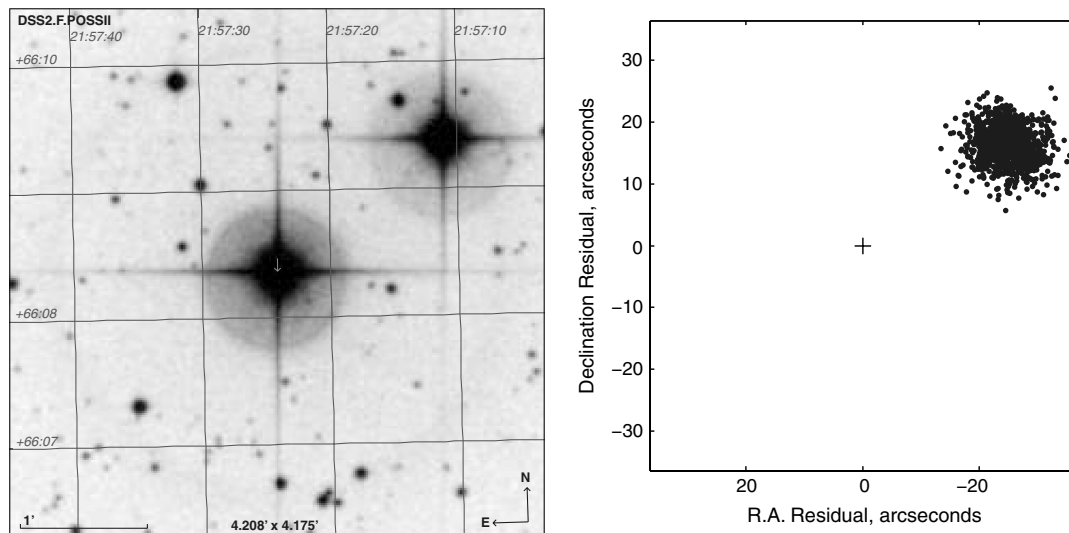

Fig. 4 SKYMAP 21570079 image (left, 250″ × 250″) and measurement residuals plot (right, 70″ × 70″). In the image, the target star is at the center and the near-neighbor to the upper right. In the residuals plot, the predicted measurement is the cross at the center and the actual measurements cluster about 20″ to the upper right. If scaled and superimposed on the image, the actual measurements cluster between the target star and the near-neighbor.

Table 4 Position residual statistics for unbiased stars grouped by tracker

Tracker	Stars	r, arcseconds	d
IST	4894	1.63 ± 0.62	0.54 ± 0.19
BST1	4378	1.20 ± 0.62	0.39 ± 0.20
BST2	4217	1.37 ± 0.64	0.46 ± 0.21

These four Aura stars were treated identically to the other 45 stars (their descriptions are based on the same standard SKY2000 catalog). They are described separately because work has been done on them for the Aura mission catalog that may be related [1]. Statistics for unbiased stars show significant performance differences between the trackers.

The objective was to study direct use of the tracker measurements for attitude estimation. Stars were identified and the resulting reference vectors from the SKY2000 catalog were used without further processing. No special processing was done for catalog information concerning double stars and variable stars. All star catalog positions and magnitudes were taken from the SKY2000 catalog. Uncertainties in the SKY2000 catalog are smaller than the ICESat tracker errors and were considered negligible. Hipparcos star identifiers were used to query astronomical databases.

A. Biased Stars

Table 2 describes 45 stars. The first two columns contain SKYMAP (SKY2000) and Hipparcos identifiers. The third column contains the number of passes. The number of passes is also the number of lower level target star pass statistics which were combined to calculate higher level star statistics. The BST passes column gives the number of target star passes measured by the BSTS. There are relatively fewer BST passes for stars with large biases. The last three columns contain higher level star statistics for the Mahalanobis distances, right ascension residuals, and declination residuals.

Table 3 describes four stars in the 2004 Aura onboard catalog. Work has been done on near-neighbors for the 3542 stars in the Aura onboard catalog [1]. The third column contains the Aura onboard catalog identifier. These four stars were processed identically to the other 45 stars and their descriptions are based on the same standard SKY2000 catalog. They are listed separately for possible comparison with Aura onboard catalog results.

Near-neighbors were visually confirmed for each of these stars using images from an astronomical database. Plots of right ascension and declination residuals confirmed that the directions and magnitudes of the residuals correlated with the positions of near-neighbors. Figure 4 is an example image and measurement residuals plot for the second star in Table 2. The cross at the center of the residuals plots is the predicted measurement. The actual measurements cluster 20 arcseconds to the upper right. If the measured positions were superimposed on the image and adjusted to the same scale, they would cluster between the target star and the near-neighbor. The variations of the measurement residuals are due to star tracker measurement noise and variations of the single-frame attitude estimates over many frames of measurements.

B. Unbiased Stars

Unbiased stars had r values less than five arcseconds and d values less than one. Statistics for large samples of unbiased stars were used to characterize the trackers. The statistics were affected by both position measurement noise and single-frame attitude estimation errors. They directly effected the measured and predicted positions in r, and they appeared in the equation for $\mathbf{S}$ and therefore d. The distributions of r and d values were described using mean values and standard deviations. Table 4 contains statistics for unbiased stars grouped by tracker. BST1 had smaller position residuals than the other two trackers.

VI. Conclusions

Attitude and pointing estimation depend on accurate measurements of star unit vectors in the tracker coordinate frame. The method described here predicts tracker position measurements using the SKY2000 star catalog and then compares the tracker measurements to the predictions. The results are estimated biases of tracker position measurements (not star catalog positions) and statistics describing the measured minus predicted position residuals.

References

[1] Sande, C., Natanson, G., and Tracewell, D., "Effects of Uncataloged Near-Neighbor Stars on CCDST Operation," *Proceedings of the NASA Goddard Flight Mechanics Symposium*, NASA CP-2005-212789, 2005.

[2] Fowell, R. A., Smith, N., Bae, S., and Schutz, B. E., "Bad Stars," *Annual AAS Rocky Mountain Conference*, AAS Paper 09-012, 2009; also *Advances in the Astronautical Sciences*, Vol. 133, pp. 20–36.

[3] Kudva, P., and Throckmorton, A., "Preliminary Star Catalog Development for the Earth Observation System AM1 (EOS-AM1) Mission," *Journal of Guidance, Control, and Dynamics*, Vol. 19, No. 6, 1996, pp. 1332–1336.
doi:10.2514/3.21790

[4] Van Bezooijen, R. W. H., Degen, L., and Nichandros, H., "Guide Star Catalog for the Spitzer Space Telescope Pointing Calibration and Reference Sensor," *SPIE Proceedings Vol. 5487, Optical, Infrared, and Millimeter Space Telescopes*, Society of Photo-Optical Instrumentation Engineers, Bellingham, WA, Oct. 2004, pp. 253–265.

[5] Lauer, M., Jauregui, L., and Kielbassa, S., "Operational Experience with Autonomous Star Trackers on ESA Interplanetary Spacecraft," *Proceedings of the 20th International Symposium on Space Flight Dynamics*, NASA CP-2007-214158, 2007.

[6] Mortari, D., Junkins, J. L., and Samaan, M. A., "Lost-In-Space Pyramid Algorithm for Robust Star Pattern Recognition," *Annual AAS Rocky Mountain Conference*, AAS Paper 01-004, 2001; also *Advances in the Astronautical Sciences*, Vol. 107, pp. 49–68.

[7] Sande, C., Ottenstein, N., Tracewell, D., and Oza, D., "SKYMAP Requirements, Functional, and Mathematical Specifications," Computer Sciences Corporation Rept. No. CSC-96-932-24, Aug. 1999.

[8] Schutz, B. E., Bae, S., Smith, N., and Sirota, J. M., "Precision Orbit And Attitude Determination For ICESat," *F. Landis Markley Astronautics Symposium* AAS Paper 08-305, June 2008; also *Advances in the Astronautical Sciences*, Vol. 132, pp. 775–791.

[9] Wu, Y.-W., and Li, R., "Star Tracker Error Characteristics and Their Compensation Techniques," *Proceedings of the NASA Goddard Flight Mechanics Symposium*, Proceedings NASA CP-2003-212246, 2003.

[10] Mortari, D., "SP-Search: A New Algorithm for Star Pattern Recognition," *Astrodynamics Specialist Conference*, AAS Paper 99-437, Aug. 1999; also *Advances in the Astronautical Sciences*, Vol. 102, pp. 1165–1174.

[11] Bae, S., Ricklefs, R., Smith, N., and Schutz, B. E., "Time Tag Issues in the Star Tracker and Gyro Data for ICESat Precision Attitude Determination," *Spaceflight Mechanics Meeting*, AAS Paper 09-128, 2009; also *Advances in the Astronautical Sciences*, Vol. 134, pp. 431–444.

[12] Smith, N., "Localized Distortion Estimation and Correction for the ICESat Star Trackers," M.S. Thesis, Aerospace Engineering Dept., Univ. of Texas, Austin, TX, 2006.

[13] Markley, F. L., "Attitude Determination using Vector Observations and the Singular Value Decomposition," *Journal of the Astronautical Sciences*, Vol. 36, No. 3, 1988, pp. 245–258.

[14] Zacharias, N., and Dorland, B., "The Concept of a Stare-mode Astrometric Space Mission," *Publications of the Astronomical Society of the Pacific*, Vol. 118, No. 848, 2006, pp. 1419–1427.
doi:10.1086/508299

D. Spencer
Associate Editor